A Robust Augmented Nodal Analysis Approach to Distribution Network Solution

O.S. Nduka, *Member, IEEE,* Y. Yu, *Student Member, IEEE,* B.C. Pal, *Fellow, IEEE,* E.N.C Okafor

***Abstract*—The ambition to decarbonize the source of energy for heat and transport sector through electricity from renewable energy has led to significant challenge in the way power distribution networks (DNs) are planned, designed and operated. Traditionally, DN was put in place to support the demand passively. Now with renewable generation, storage and demand side management through automation, provision of network support services have transformed the character of the DNs. Active management of the DN requires fast power flow analysis, state estimation, reactive power support etc. This paper proposes a method of power flow analysis which incorporates the challenges of distributed generator (DG) characteristics, demand side management and voltage support. The proposed approach reformulated the Jacobian matrix of the well-known modified augmented nodal analysis (MANA) method; thus, improving the robustness and solvability of the formulation. Reactive powers of the DGs, node voltages and currents of 'non-constitutive' elements were the chosen state variables. The performance of this method is compared with the MANA. Results are discussed and the effectiveness of the proposed approach is demonstrated with two example case studies.**

***Index Terms*—Voltage control, modified augmented nodal analysis, decarbonisation, distributed generator, stressed network, power flow analysis, modelling, smart grid**

I. Introduction

DECARBONIZATION of the energy sector has led to growth of low carbon technology such as photovoltaics, wind and energy storage systems integration into the power distribution networks. Such technologies are mainly localized in nature; hence they have significant impacts on the operating characteristics of low voltage network. Forecasts suggest that transporting the energy demand of the heat and transport sectors will require a robust power distribution delivery infrastructure [1]. In fact, it is predicted that with high electrification of the transport sector, the electricity consumption will increase by $50 - 135\%$ in 2050 than the existing levels [2].

Research has also shown that load demand is growing at a faster pace than network infrastructure expansion. In [3], the International Energy Agency (IEA) projected that load growth in the year 2020 will be 12% higher than estimates in 2010. On the other hand, network asset expansion has been projected to be 6% [4]. This has resulted in increased awareness of the need for demand side management approach for optimum operation of the network [1].

This work was funded by the Joint UK-India Clean Energy (JUICE) project, EP/P003605/1.

O. S. Nduka, Y. Yu and B. C. Pal are with the Control and Power Research Group, Electrical and Electronic Engineering Department, Imperial College, London SW7 2AZ, U.K. (e-mail: on212@ic.ac.uk; b.pal@imperial.ac.uk)

E.N.C Okafor is with the Federal University of Technology, Owerri, Imo State, Nigeria (ephraimnc.okafor@futo.edu.ng).

An example of demand side management technique is the use of DGs for providing active and reactive power support and hence voltage control [5]. Both distributed and centralised control of the DGs for this purpose already exist in several European networks. One way the DGs regulate the voltage is through the control of reactive power injected (absorbed) to (from) the network by the power converter of the DGs [6].

Generally power flow analysis is the starting point for implementation of such controls. Obviously, several power flow methods exist. Well-known methods such as Gauss-Seidel, Newton-Raphson and fast-decoupled methods are known to converge well for the traditional transmission networks [7]. However, such methods do not perform optimally when applied to distribution systems [8]. This is due to the characteristics of typical DNs such as high R/X ratio, untransposed lines and radial topology. Also, a very important reason for divergence is the presence of zero impedance paths (due to closed switches) which are common in DNs [9], [10]. It is well known that a closed switch is usually modelled as a short-circuit which implies zero impedance. Consequently, the admittance of that branch will approach infinity. Having an infinite entry in the Jacobian matrix often results in ill-conditioning and consequently leading to divergence. A way around representation of switches in the literature is to eliminate the closed switch portion i.e. merge the two interconnecting nodes or represent the switch impedance with very small value. Such alternative methods introduce errors [9].

Nevertheless, methods that work well for distribution systems have also been developed. These include the current injection methods (CIM) and their variants [11]–[15] and the forward-backward sweep technique [16], [17]. While the underlying principles (network equations and power balance/conservation constraints) used in the model formulation for a category of power flow analysis method remains the same, the consideration of practical network conditions result in the improved variants. For instance, in [17], the difficulty of accurately and explicitly representing transformer models in the classical forward/backward sweep method was addressed.

In [18], the model for centre-tapped transformer was developed and integrated into the backward-forward scheme for simulation. Similarly, [12] extended the single-phase CIM power flow calculations presented in [11] to three-phase analysis. Ref. [19] has also proposed models for thyristor-controlled series compensators and voltage-controlled devices. Other methods of power flow calculations include the loop impedance methods [20] and optimisation-based approaches - using conic programming [21] and primal dual interior point methods [22].

Despite their strengths, some of the distribution network power flow methods diverge under certain practical network conditions. For instance, the CIM proposed in [12] failed to converge for a stressed network with several voltage controlled nodes. This led to development of an improved current injection method (ICIM) [23]. The authors suggested that the technique used for dealing with voltage controlled constraints could have resulted to the divergence of the CIM approach.

Recently, the modified nodal analysis was extended to the study of power flows in multi-phase distribution networks thus yielding the "modified augmented nodal analysis (MANA)" method [24]. The MANA technique was also used for distribution system state estimation in [10]. Additionally, an extension of the MANA technique was used in the assessment of harmonics [25], [26]. The modified nodal analysis and its variants are indeed very powerful computational tools due to the following reasons: ability to accommodate all kinds of network component models (including ideal voltages and switches), amenable to system topology, permit the use of p.u or actual values and uses equations that reflect physical laws [27].

At this stage, it is pertinent to highlight that the MANA method is different from the ICIM method. First, MANA techniques generally consider not only voltages but also currents of 'non-constitutive elements' (NNEs) as state variables unlike the ICIM. The term NNEs refers to network components with current expressions that are not easily written as functions of their terminal voltages alone [27]–[29]. The addition of current variables is what resulted to the name in the literature - modified nodal analysis [27], [29].

Furthermore, DG control of node voltages could be implemented remotely or in localized manner. Remote control of node voltages using the on-load tap changer transformer, regulators and capacitors was considered in [24]. However, similar to classical network power flow methods, the voltage controlled (PV-type) nodes were modelled by replacing the reactive power (Q) formulations with the voltage constraint equations in the MANA [10], [24].

As argued in [23], that approach resulted in divergence for distribution networks operating under stress and having voltage control requirement. This convergence issue for stressed network with voltage regulation is likely to be the case for MANA too, as this paper will demonstrate later. The reason for the divergence is that the voltage constraint equation and the linearisation (with voltage mismatch set to zero) hold true if and only if convergence has been achieved. Thus, substituting that for Q-formulation when convergence has not been achieved results in ill-conditioned formulation.

Another identified challenge when MANA and other Newton-Raphson based techniques are deployed for the power flow studies is that of initialization. While the nodal voltages have always been initialized with flat voltage start (1p.u) estimates [30], initializing and updating of the reactive powers pose a challenge to the convergence guarantee [31]. Consequently, tuning for the reactive power variable is generally required to achieve convergence.

In this work, we seek to reformulate the MANA in order to eliminate the need for tuning [30], [31]. As the method results in useful improvement of the MANA, it is referred to as enhanced modified augmented nodal analysis (EMANA) technique. Specifically, the enhancement to the MANA formulation was achieved by including the reactive powers of DGs as state variables in addition to currents and voltages. The Jacobian matrix was thereafter rewritten with additional three block matrices introduced. The constructed Jacobian matrix and hence the formulation is thus well-conditioned and therefore shows improved solvability and robustness when stressed medium voltage distribution networks (MVDNs) with local voltage regulation requirements from DGs is assessed.

Two practical European MVDN with DGs providing voltage regulation ancillary services have been simulated. The performances of the classical MANA and the proposed EMANA have been compared based on the simulation results. The robustness of EMANA is clearly demonstrated based on two indices namely - impact of initial iterates and its updating on the convergence guarantee and the condition number. This improved solvability and robustness is indeed a useful improvement of the MANA technique.

The second objective of this paper is to provide a detailed mathematical formulation of the MANA and EMANA methods in order to encourage its wide adoption by researchers and power systems analysis software developers.

Other sections of this paper are organised as follows: Section II provides an explicit formulation and discussion of the MANA technique whereas Section III presents the proposed EMANA approach. Also, Section IV provides an application of the proposed method to test power systems and the results discussed. This is then followed by the concluding remarks.

II. Explicit discussion on the MANA technique

As stated previously, the MANA is a reliable method for power systems analysis. For gentle introduction to the modified nodal analysis technique, readers are referred to [27]. For purpose of clarity, the classical MANA will be discussed before presentation of the proposed EMANA.

A. Single phase MANA analysis

From the power systems perspective, the MANA approach can be summarised for a single-phase network as (1).

$$F_G(X) = \left[Y_{(AugStamp)}\right][X]+[I]_{A_{(PQ)}}-[I]_{A_{(gen)}}-[W] = [0] \tag{1}$$

where:

$$\left[Y_{(AugStamp)}\right] = \underset{\epsilon\mathbb{C}^{(N+P_N)\times(N+P_N)}}{\begin{bmatrix} \left[Y_{(Stamp)}\right] & \begin{bmatrix}A\end{bmatrix} \\ \begin{bmatrix}B\end{bmatrix} & \begin{bmatrix}C\end{bmatrix} \end{bmatrix}} \tag{2}$$

$$[X] = \begin{vmatrix} [V_n] \\ [I_{nne}] \end{vmatrix}; [W] = \begin{vmatrix} [I_{(is)}] \\ [V_{(is)}] \end{vmatrix} \tag{3}$$

$$\begin{aligned} [V_n] &= \begin{bmatrix} V_1 & V_2 & \dots & V_N \end{bmatrix}^T; \\ [I_{(nne)}] &= \begin{bmatrix} I_{(p_1)} & I_{(p_2)} & \dots & I_{(p_N)} \end{bmatrix}^T \end{aligned} \tag{4}$$

$$[I]_{A_{(PQ)}} = \begin{vmatrix} I_{(pq)_1} \\ I_{(pq)_2} \\ \vdots \\ I_{(pq)_N} \\ [O]_{(P_N \times 1)} \end{vmatrix}; [I]_{A_{(gen)}} = \begin{vmatrix} I_{(gen)_1} \\ I_{(gen)_2} \\ \vdots \\ I_{(gen)_N} \\ [O]_{(P_N \times 1)} \end{vmatrix} \tag{5}$$

$$\begin{aligned} [I_{(is)}] &= \begin{bmatrix} I_{(p)_1} & I_{(p)_2} & \dots & I_{(p)_N} \end{bmatrix}^T; \\ [V_{(is)}] &= \begin{bmatrix} V_{(p)_1} & V_{(p)_2} & \dots & V_{(p)_{P_N}} \end{bmatrix}^T \end{aligned} \tag{6}$$

$$[Y_{stamp}] = \begin{bmatrix} \ddots & & & & \\ & [Y_{ii}] & \dots & [Y_{ik}] & \\ & \vdots & \vdots & \vdots & \\ & [Y_{ki}] & \dots & [Y_{kk}] & \\ & & & & \ddots \end{bmatrix}_{(l+cap.+yload)} \epsilon \mathbb{C}^{N \times N} \tag{7}$$

For the purpose of clarity, the term $[I]_{A_{(PQ)}}$ and $[I]_{A_{(gen)}}$ are augmented vector of currents for PQ load and generator nodes. Also, subscripts (nne), N, n, (p) and P_N refer to terms associated with the NNEs, the total number of nodes in the system, node index, independent source index, and the total number of NNE currents respectively. Subscript (is) denotes independent source. $[A]$, $[B]$ and $[C]$ are the block matrices derived from the voltage and current constitutive equations and the associated impedance matrix of the NNE. The NNEs in this contexts are network components whose currents are difficult to write as functions of node voltages alone. Lastly, [W] is the vector of independent current and voltage sources.

Generally in the above formulation (1), the slack bus is modelled as a voltage source and is therefore embedded accordingly. Also note that only PQ load current has been shown in (1); this is because the constant impedance loads were directly included in the $[Y_{stamp}]$ matrix. The formulation takes into account all possible load types (impedance, power or current) and configurations (delta or star arrangements). The linear elements are directly 'stampedâĂŹ into the matrix $[Y_{stamp}]$ similar to classical nodal analysis [27].

Consider for instance that a single-phase PQ load is connected at node '2' whereas a distributed generator (1-phase) is connected at node '3', then the $[I]$ term can be written as follows:

$$\begin{aligned} I_{pq2} &= \frac{1}{|V_2|^2}\left(P_{pq2}V_2^x + Q_{pq2}V_2^y + j\left(P_{pq2}V_2^y - Q_{pq2}V_2^x\right)\right) \\ I_{gen3} &= \frac{1}{|V_3|^2}\left(P_{g3}V_3^x + Q_{g3}V_3^y + j\left(P_{g3}V_3^y - Q_{g3}V_3^x\right)\right) \end{aligned} \tag{8}$$

$$|V_k| = \sqrt{(V_k^x)^2 + (V_k^y)^2}; \quad k\epsilon\{2,3\} \tag{9}$$

The superscripts x and y respectively denote the real and imaginary terms. For the case of voltage controlled (PV-type) node, the Q row of PQ control expression in the Jacobian matrix is replaced by the voltage constraint equation [24]. If this node is i^{th} node, then the voltage constraint is as given in (10).

$$F_{pv}(V_n) = |V_i|^2 - (V_i^x)^2 - (V_i^y)^2 = 0 \tag{10}$$

The MANA formulation generally reduces to a direct method when only impedance loads are considered but requires an iterative procedure when nonlinear current expressions (e.g. due to PQ loads or presence of distributed generators) are involved. The direct method is not mentioned beyond this point.

The Newton-Raphson iterative procedure required to solve the formulation in (1) can be realised as shown in (11).

$$\begin{aligned} \left[(\triangle X)\right]^{(b)} &= -\left[(ON)^{(b)}\right]^{-1}\left[F_G(X)\right]^{(b)} \\ \left[X\right]^{(b+1)} &= \left[X\right]^{(b)} + \left[(\triangle X)\right]^{(b)} \end{aligned} \tag{11}$$

where:

$$\left[F_G(X)\right]^{(b)} = \underbrace{\left(\left[Y_{(AugStamp)}\right][X] + [I]_{Aug} - [W]\right)^{(b)}}_{\epsilon \mathbb{R}^{2(N+P_N)}} \tag{12}$$

$$\left[(X)\right] = \begin{bmatrix} [V_n] & [I_{(p)_{sl}}] & [I_{(p)_n}] & [I_{(p)_l}] \end{bmatrix}^T \tag{13}$$

$$[I]_{Aug} = [I]_{A_{(PQ)}} - [I]_{A_{(gen)}} \tag{14}$$

The term $[ON]$ is the Jacobian matrix which is represented as shown in (15).

$$\left[ON\right] = \begin{bmatrix} [S] & [A]_{sl} & [A]_n & [A]_l \\ [B]_{sl} & [C]_{(zsl)} & & \\ [B]_n & & [C]_{(zn)} & \\ [B]_l & & & [C]_{(zl)} \end{bmatrix} \tag{15}$$

$$[S] = \left(\left[Y_{(Stamp)}\right] + [ON]_{(PQ)_n} - [ON]_{(gen)_n}\right) \tag{16}$$

Note that the subscripts sl, n, l represent the terms associated with the slack, node and line components. In particular, $[B]_l$ and $[A]_l$ are the block matrices derived from the voltage and current constitutive equations for a line-type NNE. $[C]_{(zl)}$ is the associated impedance matrix. An example for such derivations is provided in the Appendix. The $[ON]$ terms in (16) can be written for the single phase case as (17) and (18)

$$[ON]_{(PQ)_n} = \text{diag}\left(\begin{vmatrix} \vdots & \\ \frac{1}{\left(\sqrt{(V_k^x)^2+(V_k^y)^2}\right)^4}\begin{bmatrix} J_{k1} & J_{k2} \\ J_{k3} & J_{k4} \end{bmatrix} \\ \vdots & \\ \frac{1}{\left(\sqrt{(V_N^x)^2+(V_N^y)^2}\right)^4}\begin{bmatrix} J_{N1} & J_{N2} \\ J_{N3} & J_{N4} \end{bmatrix} \end{vmatrix}\right)_{(PQ)_n} \tag{17}$$

where:

$$[ON]_{(gen)_n} = \text{diag}\left(\begin{vmatrix} \vdots & \\ \frac{1}{\left(\sqrt{(V_i^x)^2+(V_i^y)^2}\right)^4}\begin{bmatrix} J_{i1} & J_{i2} \\ J_{i3} & J_{i4} \end{bmatrix} \\ \vdots & \\ \frac{1}{\left(\sqrt{(V_N^x)^2+(V_N^y)^2}\right)^4}\begin{bmatrix} J_{N1} & J_{N2} \\ J_{N3} & J_{N4} \end{bmatrix} \end{vmatrix}\right)_{(gen)_n} \tag{18}$$

where the terms $J_{k1}, \ldots, J_{k4}, J_{i1}, \ldots, J_{i4}$ are as defined in the Appendix. A change in domain from complex to real was used in order to implement the Newton-Raphson iterative technique. For clarity, the 'unaugmented stampedâĂŹ admittance matrix $[Y_{Stamp}]$ in (7) is translated into reals using (19).

$$[Y_{stamp}] = \begin{bmatrix} \ddots & & & & \\ & \begin{bmatrix} Y_{ii}^{y} & Y_{ii}^{x} \\ Y_{ii}^{x} & -Y_{ii}^{y} \end{bmatrix} & \cdots & \begin{bmatrix} Y_{ik}^{y} & Y_{ik}^{x} \\ Y_{ii}^{x} & -Y_{ik}^{y} \end{bmatrix} & \\ & \vdots & \vdots & \vdots & \\ & \begin{bmatrix} Y_{ki}^{y} & Y_{ki}^{x} \\ Y_{ki}^{x} & -Y_{ki}^{y} \end{bmatrix} & \cdots & \begin{bmatrix} Y_{kk}^{y} & Y_{kk}^{x} \\ Y_{kk}^{x} & -Y_{kk}^{y} \end{bmatrix} & \\ & & & & \ddots \end{bmatrix}_{\epsilon \mathbb{R}^{2N \times 2N}} \tag{19}$$

Obviously, the term Y_{ii}^{y} and Y_{ii}^{x} in (19) respectively denote the imaginary (susceptance) and real (conductance) of the admittance. The above formulation can be coded in any software platform and simulated for any network topology either using actual values or the p.u. In this technical work, MATLAB has been used for all coding and simulations. The actual values were used for all simulations and analyses in this paper.

B. Three-phase MANA analysis

The three-phase MANA technique can be developed following similar approach as presented for the single-phase analysis discussed in the previous subsection. However, the mutual cross-couplings and untransposed lines must be accounted for where they exist in the test power network. Additionally, inherent system imbalance as well as load imbalance must be considered.

Similar to the single-phase analysis, the formulation in (11) can be modified for the 3-phase and solved iteratively to obtain the system state variables. For example, in the 3-phase analysis, the matrix $[Y_{Stamp}]$ would be written as in (20).

$$[Y_{stamp}]^{(abc)} = \begin{bmatrix} \ddots & & & & \\ & \begin{bmatrix} Y_{ii}^{y} & Y_{ii}^{x} \\ Y_{ii}^{x} & -Y_{ii}^{y} \end{bmatrix}^{(abc)} & \cdots & \begin{bmatrix} Y_{ik}^{y} & Y_{ik}^{x} \\ Y_{ii}^{x} & -Y_{ik}^{y} \end{bmatrix}^{(abc)} & \\ & \vdots & \vdots & \vdots & \\ & \begin{bmatrix} Y_{ki}^{y} & Y_{ki}^{x} \\ Y_{ki}^{x} & -Y_{ki}^{y} \end{bmatrix}^{(abc)} & \cdots & \begin{bmatrix} Y_{kk}^{y} & Y_{kk}^{x} \\ Y_{kk}^{x} & -Y_{kk}^{y} \end{bmatrix}^{(abc)} & \\ & & & & \ddots \end{bmatrix}_{\epsilon \mathbb{R}^{6N \times 6N}} \tag{20}$$

where:

$$\begin{bmatrix} Y_{ii}^{y} & Y_{ii}^{x} \\ Y_{ii}^{x} & -Y_{ii}^{y} \end{bmatrix}^{(abc)} = \begin{bmatrix} \begin{bmatrix} Y_{ii}^{aay} & Y_{ii}^{aby} & Y_{ii}^{acy} \\ Y_{ii}^{bay} & Y_{ii}^{bby} & Y_{ii}^{bcy} \\ Y_{ii}^{cay} & Y_{ii}^{cby} & Y_{ii}^{ccy} \end{bmatrix} & \begin{bmatrix} Y_{ii}^{aax} & Y_{ii}^{abx} & Y_{ii}^{acx} \\ Y_{ii}^{bax} & Y_{ii}^{bbx} & Y_{ii}^{bcx} \\ Y_{ii}^{cax} & Y_{ii}^{cbx} & Y_{ii}^{ccx} \end{bmatrix} \\ \begin{bmatrix} Y_{ii}^{aax} & Y_{ii}^{abx} & Y_{ii}^{acx} \\ Y_{ii}^{bax} & Y_{ii}^{bbx} & Y_{ii}^{bcx} \\ Y_{ii}^{cax} & Y_{ii}^{cbx} & Y_{ii}^{ccx} \end{bmatrix} & - \begin{bmatrix} Y_{ii}^{aay} & Y_{ii}^{aby} & Y_{ii}^{acy} \\ Y_{ii}^{bay} & Y_{ii}^{bby} & Y_{ii}^{bcy} \\ Y_{ii}^{cay} & Y_{ii}^{cby} & Y_{ii}^{ccy} \end{bmatrix} \end{bmatrix}_{\epsilon \mathbb{R}^{6 \times 6}} \tag{21}$$

In the same vein,

$$\left[(X)\right]^{(abc)} = \begin{vmatrix} [V_n]^{(abc)} \\ [I_{(p)_{sl}}]^{(abc)} \\ [I_{(p)_n}]^{(abc)} \\ [I_{(p)_l}]^{(abc)} \end{vmatrix}; \quad [V_n]^{(abc)} = \begin{vmatrix} [V_1]^{(abc)} \\ [V_2]^{(abc)} \\ [V_3]^{(abc)} \\ \vdots \\ [V_N]^{(abc)} \end{vmatrix} \tag{22}$$

where as an example,

$$[V_k]^{(abc)} = \begin{bmatrix} V_k^{ax} & V_k^{bx} & V_k^{cx} & V_k^{ay} & V_k^{by} & V_k^{cy} \end{bmatrix}^T \tag{23}$$

For the purpose of simplicity, consider that the load configuration in the 3-phase network is grounded wye, then the Jacobian submatrix for PQ term, $[ON]_{(PQ)_n}^{(abc)}$, in the 3-phase analysis can be derived as presented in (24). It is important to state that other load configurations (delta, or ungrounded wye) are also easy to include in the formulation but have not been shown due to space limitation.

$$[ON]_{(PQ)_n}^{(abc)} = \text{diag}\left(\begin{bmatrix} & \vdots & \\ \cdots & \begin{bmatrix} H_{i1} & H_{i2} \\ H_{i3} & H_{i4} \end{bmatrix} & \cdots \\ & \vdots & \\ \cdots & \begin{bmatrix} H_{k1} & H_{k2} \\ H_{k3} & H_{k4} \end{bmatrix} & \cdots \\ & \vdots & \end{bmatrix} \right)_{\epsilon \mathbb{R}^{6N \times 6N}} \tag{24}$$

where terms in (24) are defined in the Appendix. Using similar approach as discussed, the remaining variables in the generalized formulation were also modified appropriately; thus, yielding a detailed phase-frame representation of the Newton-Raphson formulation for the 3-phase MANA.

III. Evolution of the EMANA

In this section, the EMANA is demonstrated. First, the previous MANA formulation was modified such that additional system state variable (DG reactive power, Q, in this case) was added for each voltage-controlled node. The Jacobian matrix was reformulated and constructed in a form that is well-conditioned. Specifically, three block matrices were introduced in the Jacobian matrix. This improved the solvability and robustness of the solution technique.

Note that although the ICIM also uses reactive power as state variables, a remarkable difference between the EMANA

and ICIM is that currents of NNEs are also solution variables in EMANA, which is generally an attribute of modified nodal analysis based methods. This implies the differences in the formulation methodology. Also, the direct calculation of the the NNEs currents eliminates the need for post-processing as it is the case when classical methods are used and the knowledge of these values required.

For illustrative purposes, the Newton-Raphson formulation for the single-phase analysis (11) was modified to (25) to include the voltage controlled constraints.

$$\big[(\triangle X)\big]^{(b)} = -\big[(ON)^{(b)}\big]^{-1}\big[F(X)\big]^{(b)} \tag{25}$$

where:

$$\big[F(X)\big]^{(b)} = \begin{vmatrix} [F_G(X)] \\ [F_{pv}(V_n)] \end{vmatrix}^{(b)} \tag{26}$$

$$[F_{PV}(V_n)]^{(b)} = \begin{vmatrix} F_{(pv)_1}(V_n) \\ F_{(pv)_2}(V_n) \\ \vdots \\ F_{(pv)_M}(V_n) \end{vmatrix}^{(b)} \epsilon\mathbb{R}^M; \tag{27}$$

$$\Rightarrow [F_{PV}(V_n)]^{(b)} = \begin{vmatrix} \vdots \\ |V_i|^2 - (V_i^x)^2 - (V_i^y)^2 \\ |V_{(i+1)}|^2 - \left(V_{(i+1)}^x\right)^2 - \left(V_{(i+1)}^y\right)^2 \\ \vdots \\ |V_M|^2 - (V_M^x)^2 - (V_M^y)^2 \end{vmatrix}^{(b)} \tag{28}$$

The new state vector for the single phase system is described as:

$$[(X)] = \big[[V_n] \quad [I_{(p)_{sl}}] \quad [I_{(p)_n}] \quad [I_{(p)_l}] \quad [Q_{(p)_{pv}}]\big]^T \tag{29}$$

M is the number of PV nodes present in the test network whereas $I_{(p)_n}$ represents the current of a NNE connected to node 'nâĂŹ. The subscripts sl and l are as initially defined. Three sub-matrices $\big([ON]_{(pv)_n}, \quad [U]_{pv}, \quad [T]_{pv}\big)$ are therefore introduced into the Jacobian matrix (see 30).

$$\big[ON\big] = \begin{bmatrix} [S] & [A]_{sl} & [A]_n & [A]_l & [U]_{pv} \\ [B]_{sl} & [C]_{(zsl)} & & & \\ [B]_n & & [C]_{(zn)} & & \\ [B]_l & & & [C]_{(zl)} & \\ [T]_{pv} & & & & \end{bmatrix} \tag{30}$$

$$[S] = \Big(\big[Y_{(Stamp)}\big] + [ON]_{(PQ)_n} - [ON]_{(gen)_n} - [ON]_{(pv)_n}\Big) \tag{31}$$

The term $[I]_{Aug}$ in (14) was adjusted to include the voltage controlled node part as expressed in (32) .

$$\big[I\big]_{Aug} = [I]_{A_{(PQ)}} - [I]_{A_{(gen)}} - [I]_{A_{(pv)}} \tag{32}$$

$$\big[U\big]_{pv} = \frac{\partial[I]_{A_{(pv)}}}{\partial[Q_{(p)_{pv}}]} \tag{33}$$

$$\big[T\big]_{pv} = \frac{\partial[F_{PV}([V_n])]}{\partial[V_n]} \tag{34}$$

Note that $[ON]_{(pv)_n}$ has the same form as (17) with the exception that the coefficients $\frac{1}{\left(\sqrt{(V_k^x)^2+(V_k^y)^2}\right)^4}$ for $k\epsilon\{1,2,\ldots,M\}$ are given for the case of (PV) nodes but V_k^x and V_k^y are unknowns.

The evolution of the 3-phase equivalent formulation for the EMANA was achieved by extending the variables similar to previous presentations for the MANA technique shown earlier. For instance, in the 3-phase analysis $[U]_{pv}$ and $[T]_{pv}$ were rewritten as presented in (35) and (36).

$$\big[U\big]_{pv}^{(abc)} = \frac{\partial\big[I\big]_{A_{(pv)}}^{(abc)}}{\partial[Q_{(p)_{pv}}]^{(abc)}} \tag{35}$$

$$\big[T\big]_{pv}^{(abc)} = \frac{\partial[F_{PV}([V_n])]^{(abc)}}{\partial[V_n]^{(abc)}} \tag{36}$$

A. Algorithm implementation

The logical sequence of operation followed in the implementation of the proposed EMANA is as detailed below.

1) Sweep through the network and identify slack, PV and PQ nodes
2) Identify all constitutive elements (NEs) and NNEs in the network
3) Form $[Y_{Stamp}]$
4) Form $[Y_{AugStamp}]$
5) Initialize state variable [X]
6) while Iter $\leq$ MaxIter and Max $\big(|\big[(\triangle X)\big]|\big) >$ Error
   a.) Compute Jacobian matrix $[ON]$
   b.) Compute [F(X)]
   c.) Solve (25)
   d.) Update state variable [X]
7) End iteration
8) Display Iteration count, Iter

IV. Application to test power networks

The capability of the proposed EMANA technique was demonstrated experimentally by the simulation of the UKGDS 95-bus and a practical Italian MVDN provided in [6]. Experimental results realised were compared as discussed here. As the Newton-Raphson iterative procedure requires initialization, we have analysed the performance of the two methods against several starting points named as flat start and tuned start. The flat start involved the use of zero reactive power values as the initial iterates for the DGs whereas the tuned start required the use of calculated or reasonable estimates (see [30]). Also in the tuned start, the reactive powers were not updated in MANA. It was realised that updating the reactive powers in both the flat and tuned starts was problematic for the MANA. This is due to the nature of the Jacobian matrix of the MANA when the PQ control is modified by the voltage constraint variable for a voltage controlled node.

The condition number of the Jacobian matrix has also been assessed i.e. where both methods converged. For Jacobian matrix [ON], the condition number can be expressed as [32]:

$$cond(\big[ON\big]) = ||[ON]|| \times ||[ON]^{-1}|| \tag{37}$$

where $||.||$ represents the matrix norm. The larger the condition number, the lesser the robustness of the formulation. In other words, the formulation is considered poorly-conditioned if the condition number is very large [32]. The useful improvement

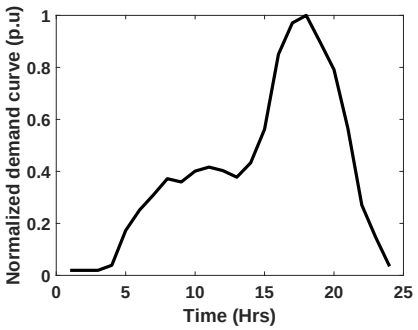

Fig. 1. Demand curve

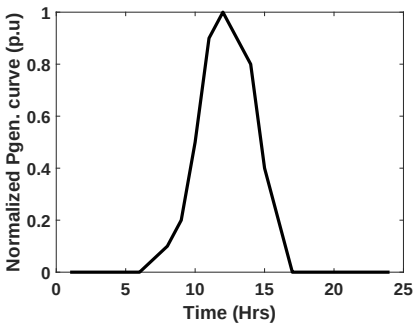

Fig. 2. Photovoltaic DG output profile

in robustness property of the EMANA in relation to MANA was revealed by evaluating the condition number of the Jacobian matrix after convergence.

The load and PV-DG output power profiles obtained from [33], [34] and used for the simulations are as shown in Fig. 1 and Fig. 2. The network diagram is as shown in Fig. IV. Four photovoltaic (PV) DGs with each having 5MVA capacity have been introduced at the following nodes of the UKGDS-95 - $\{18, 37, 89 \quad \text{and} \quad 92\}$ for voltage control. The choice of 4-DGs is arbitrary while the locations of the DGs have been selected with respect to the nodes with high demand in the test distribution network. Similarly, six DGs were introduced in the Italian network. Owing to space limitations, only the UKGDS-95 network simulations are discussed.

First, the simulation was carried out with all nodes except the slack bus considered as PQ-type. Obviously, the flat start was used in this case and the load profile curve was varied between 0.2-3.2 pu loading factor for both methods and convergence was achieved for both techniques.

Next, the voltage controlled nodes were considered in the simulation with flat start initialization used. It was realised that the MANA did not converge for any of the above loading factors whereas the EMANA did as summarised in Table I. Indeed, the results in Table I assessed the convergence or divergence of the MANA and EMANA for flat voltage start and with zero DG reactive power initial estimates while enforcing the voltage support requirements from the DGs.

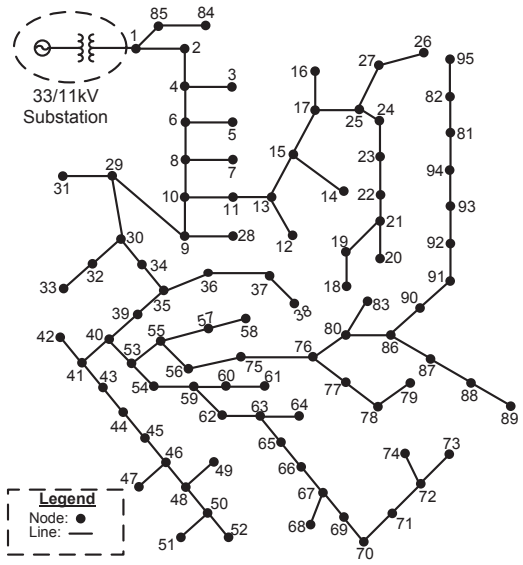

Fig. 3. UKGDS-95 test MV power system

The DG reactive powers were not tuned but rather updated alongside the nodal voltage variables after each iteration. As shown from the table, the MANA diverged under this circumstance unlike the EMANA where convergence was realised. Next, the tuned reactive power was used and the

TABLE I
SIMULATION FOR NETWORK WITH PV-NODES USING FLAT START ITERATES

Loading factor (LF)	MANA	EMANA
0.2	diverged	converged
0.5	diverged	converged
0.7	diverged	converged
1.0	diverged	converged
1.4	diverged	converged
1.8	diverged	converged
2.2	diverged	converged
⋮	⋮	⋮
3.0	diverged	converged
3.2	diverged	converged

simulation for voltage controlled case repeated. This time, both the MANA and the EMANA converged as summarised in Table II. This clearly confirmed the need for tuning of the DG reactive powers for the case of MANA. Such tuning was not required for the EMANA.

Furthermore, investigating the condition number of the Jacobian matrix revealed that this performance index was larger for MANA than EMANA by a factor of over 1000 for most cases. In fact, for the 3.2pu loading, the condition number of the Jacobian matrix of the MANA technique was 2.1×10^5 times that of the EMANA. This clearly confirmed that the EMANA is better-conditioned and hence offers useful improvement on the MANA. Moreover, as was realised from the simulation, the convergence of the EMANA does not depend on tuning of the DG reactive power values.

Fig. 4 shows a pictorial representation of the difference between MANA and EMANA in the context of the DG reactive powers. Furthermore, we have compared the performance of

TABLE II
SIMULATION FOR NETWORK WITH PV-NODES USING TUNED START ITERATES

Loading factor (LF)	MANA	EMANA
0.2	converged	converged
0.5	converged	converged
0.7	converged	converged
1.0	converged	converged
1.4	converged	converged
1.8	converged	converged
2.2	converged	converged
⋮	⋮	⋮
3.0	converged	converged
3.2	converged	converged

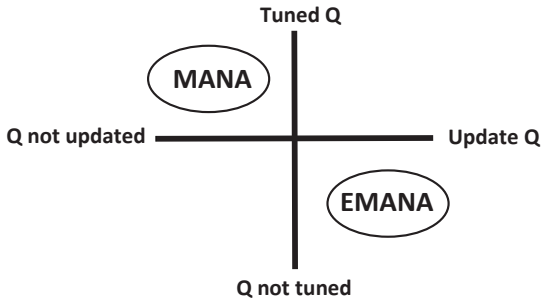

Fig. 4. Pictorial representation showing difference between MANA and EMANA in the context of DG reactive power

EMANA and MANA also in terms of the computation time. It was realised that EMANA performed better than the MANA with regards to the CPU runtime. Particularly, for a loading factor of 3.2p.u, the time taken to achieve convergence for the MANA and EMANA were respectively 0.12 and 0.07 seconds. Indeed, the speed of simulation is heavily dependent on the programming ability of the authors âĂŞ a highly skilled software developer might achieve convergence in a shorter time for example if the codes are written in C programming language.

In comparison with traditional Newton-Raphson (NR) formulation, when convergence was achieved, the NR converged faster and in fewer iterations than the MANA and EMANA. It is important to state that both MANA and EMANA also use the NR iterative scheme. The classical NR been faster than MANA and EMANA is not surprising since it computed fewer variables than the other two methods (MANA and EMANA). On closer assessment, this is not a disadvantage in the true sense as some of the variables (such as transformer, slack bus and closed switch currents which are usually present in typical test distribution networks) are directly computed from MANA and EMANA but will require further post-processing to be obtained where classical NR method is used. Moreover, [23] has already demonstrated the inability of traditional NR to converge for stressed distribution networks with voltage regulation requirement. Other cases and test networks where classical NR diverged are also discussed in [30].

Indeed, both MANA and EMANA are based on physical laws (and not just mathematical abstraction) which is an advantage. Summarily, as the ICIM is to CIM [23], so is EMANA to MANA.

A. Discussions on EMANA versus MANA

Indeed, the improved solvability and robustness of EMANA is associated with how the reactive power (control variable) of the DG is handled in the formulation. While the voltage components (V_x, V_y) and currents (I_x, I_y) and the reactive powers of the DGs are the state variables in the proposed EMANA, the MANA uses the imaginary component of voltage (V_y), current components (I_x, I_y) and the reactive power of DGs. The real component of the voltage is eliminated based on substitution with the following equation for PV (voltage controlled) nodes: $V_x^2 = V^2 - V_y^2$. However, [23] has already proven that this constraint and its linearization (with the voltage mismatch set to zero) are true at the point when convergence has been achieved. We believe this is the reason for divergence in the MANA when the reactive power is not tuned.

Concerning the improved solvability and robustness, the resulting Jacobian matrix realised from EMANA was more stable and less sensitive to numerical operations and thus performed better than the MANA. This was verified using condition number analysis. A brief explanation and an example on the use of condition number for the assessment of solvability and robustness has been provided in the Appendix. To demonstrate the differences between the two methods in the context of modelling of the DG voltage-controlled node, a section detailing how this is achieved for both methods has been added to Appendix.

V. CONCLUSION

In this paper, a method with an useful improvement on the well-known MANA has been presented. The method involved the reformulation of the MANA to a well-conditioned equivalent in the context of a MVDN operating under stress and with DGs providing ancillary voltage support services. Specifically, the reactive powers of the DGs were introduced as additional state variable in addition to the usual current and voltage variables used in the classical MANA. Three block matrices were introduced for PV nodes in the network and the Jacobian matrix constructed in a fashion that led to well-conditioned formulation. Consequently, improved solvability and convergence robustness were achieved for a stressed MVDN with several DG integrated and providing voltage ancillary services. With the proposed method, the bottleneck associated with tuning during updating of the reactive powers of the DGs in MANA is completely avoided. Moreover, this robustness demonstrated by the proposed method could be very useful when the technique is deployed for distribution network state estimation.

APPENDIX

A. Condition number analysis

The use of condition number in the assessment of stability and sensitivity of a matrix (representing a linear system) to changes in mathematical operations is well-known [32], [35], [36]. Consider the general expression below:

$$[A]X = B \tag{38}$$

Consider that $[A]\epsilon\mathbb{R}^{N\times N}$, ie a square matrix; X has a unique solution if $[A]$ is full-rank. For $B \neq 0$, and $[A]$ singular (i.e. $det([A]) = 0$), no solution exists if B is not in the range of [A] [36].

In practice, the condition number assesses how close the $[A]$ matrix is to been singular. If $[A]$ is indeed singular, then the $cond([A])$ will give a theoretically infinite value. For an ill-conditioned $[A]$ matrix, the condition number will be relatively large. On the other hand, a relatively small condition number suggests the [A] matrix is well-conditioned.

As an illustration, we computed the condition number in MATLAB for three different $[A]$ matrices, $[A_1]$, $[A_2]$ and $[A_3]$ as: 1, $10,000$ and ∞ respectively. where

$$[A_1] = \begin{bmatrix} 1 & 0 \\ 0 & 1 \end{bmatrix}; [A_2] = \begin{bmatrix} 1 & 0 \\ 0 & 0.0001 \end{bmatrix}; [A_3] = \begin{bmatrix} 1 & 0 \\ 0 & 0 \end{bmatrix} \quad (39)$$

Clearly, the formulation in (38) is more robust and solvable for $[A] = [A_1]$ than for $[A] = [A_2]$ or $[A] = [A_3]$. In summary, $[A] = [A_3]$ does not have an inverse since $[A_3]$ is singular and there are none or several solutions for $[A] = [A_3]$ (depending on the nature of B) [37].

B. Definition of terms

$$\begin{aligned} J_{k1} &= -2P_{k_{PQ}}V_k^xV_k^y - Q_{k_{PQ}}\left(V_k^y\right)^2 + Q_{k_{PQ}}\left(V_k^x\right)^2 \\ J_{k2} &= P_{k_{PQ}}\left(V_k^x\right)^2 - P_{k_{PQ}}\left(V_k^y\right)^2 + 2Q_{k_{PQ}}V_k^xV_k^y \\ J_{k3} &= P_{k_{PQ}}\left(V_k^y\right)^2 - P_{k_{PQ}}\left(V_k^x\right)^2 - 2Q_{k_{PQ}}V_k^xV_k^y \\ J_{k4} &= J_{k1} \end{aligned} \quad (40)$$

$$\begin{aligned} J_{i1} &= -Q_{k_{gen}}\left(V_i^y\right)^2 - 2P_{i_{gen}}V_i^xV_i^y + Q_{k_{gen}}\left(V_i^x\right)^2 \\ J_{i2} &= P_{i_{gen}}\left(V_i^x\right)^2 + 2Q_{i_{gen}}V_i^xV_i^y - P_{i_{gen}}\left(V_i^y\right)^2 \\ J_{i3} &= P_{i_{gen}}\left(V_i^y\right)^2 - P_{i_{gen}}\left(V_i^x\right)^2 - 2Q_{i_{gen}}V_i^xV_i^y \\ J_{i4} &= J_{i1} \end{aligned} \quad (41)$$

$$H_{i1} = \begin{bmatrix} \frac{1}{(\alpha_i^a)^4}J_{ia}^{yx} & 0 & 0 \\ 0 & \frac{1}{(\alpha_i^b)^4}J_{ib}^{yx} & 0 \\ 0 & 0 & \frac{1}{(\alpha_i^c)^4}J_{ic}^{yx} \end{bmatrix} \quad (42)$$

$$H_{i2} = \begin{bmatrix} \frac{1}{(\alpha_i^a)^4}J_{ia}^{yy} & 0 & 0 \\ 0 & \frac{1}{(\alpha_i^b)^4}J_{ib}^{yy} & 0 \\ 0 & 0 & \frac{1}{(\alpha_i^c)^4}J_{ic}^{yy} \end{bmatrix} \quad (43)$$

$$H_{i3} = \begin{bmatrix} \frac{1}{(\alpha_i^a)^4}J_{ia}^{xx} & 0 & 0 \\ 0 & \frac{1}{(\alpha_i^b)^4}J_{ib}^{xx} & 0 \\ 0 & 0 & \frac{1}{(\alpha_i^c)^4}J_{ic}^{xx} \end{bmatrix} \quad (44)$$

$$H_{i4} = \begin{bmatrix} \frac{1}{(\alpha_i^a)^4}J_{ia}^{xy} & 0 & 0 \\ 0 & \frac{1}{(\alpha_i^b)^4}J_{ib}^{xy} & 0 \\ 0 & 0 & \frac{1}{(\alpha_i^c)^4}J_{ic}^{xy} \end{bmatrix} \quad (45)$$

$$\begin{aligned} \alpha_i^a &= \sqrt{(V_i^{ax})^2 + (V_i^{ay})^2} \\ J_{ia}^{yx} &= -\left(2P_{i_{pq}}^a V_i^{ax}V_i^{ay} + Q_{i_{pq}}^a\left((V_i^{ay})^2 - (V_i^{ax})^2\right)\right) \\ J_{ia}^{yy} &= P_{i_{pq}}^a\left((V_i^{ax})^2 - (V_i^{ay})^2\right) + 2Q_{i_{pq}}^a V_i^{ax}V_i^{ay} \\ J_{ib}^{yx} &= -\left(2P_{i_{pq}}^b V_i^{bx}V_i^{by} + Q_{i_{pq}}^b\left((V_i^{by})^2 - (V_i^{bx})^2\right)\right) \\ J_{ib}^{yy} &= P_{i_{pq}}^b\left((V_i^{bx})^2 - (V_i^{by})^2\right) + 2Q_{i_{pq}}^b V_i^{bx}V_i^{by} \\ J_{ic}^{yx} &= -2P_{i_{pq}}^c V_i^{cx}V_i^{cy} - Q_{i_{pq}}^c\left((V_i^{cy})^2 - (V_i^{cx})^2\right) \\ J_{ic}^{yy} &= P_{i_{pq}}^c\left((V_i^{cx})^2 - (V_i^{cy})^2\right) + 2Q_{i_{pq}}^c V_i^{cx}V_i^{cy} \\ J_{ia}^{xx} &= P_{i_{pq}}^a\left((V_i^{ay})^2 - (V_i^{ax})^2\right) - 2Q_{i_{pq}}^a V_i^{ax}V_i^{ay} \\ J_{ib}^{xx} &= P_{i_{pq}}^b\left((V_i^{by})^2 - (V_i^{bx})^2\right) - 2Q_{i_{pq}}^b V_i^{bx}V_i^{by} \\ J_{ic}^{xx} &= P_{i_{pq}}^c\left((V_i^{cy})^2 - (V_i^{cx})^2\right) - 2Q_{i_{pq}}^c V_i^{cx}V_i^{cy} \\ J_{ia}^{xy} &= J_{ia}^{yx}; \quad J_{ib}^{xy} = J_{ib}^{yx}; \quad J_{ic}^{xy} = J_{ic}^{yx} \end{aligned} \quad (46)$$

C. Example NNE modelling

This subsection is aimed at improving the clarity of this method. Two NNEs (slack bus represented as a voltage source) and a 3-phase transformer bank with delta-grounded wye arrangement are presented. The latter is in this group (NNEs) because of the winding currents derivation, e.g currents in a centre-tapped transformer [18]. For the slack bus, assume that it is modelled as a voltage source with series impedance, then the following derivations were achieved as shown in (47).

$$\begin{aligned} \left[V_{sl}^{abcx}\right] - \left[Z_{sl}^{abcy}\right]\left[I_{sl}^{abcy}\right] + \left[Z_{sl}^{abcx}\right]\left[I_{sl}^{abcx}\right] &= \left[E_g^{abcx}\right] \\ \left[V_{sl}^{abcy}\right] + \left[Z_{sl}^{abcy}\right]\left[I_{sl}^{abcx}\right] + \left[Z_{sl}^{abcx}\right]\left[I_{sl}^{abcy}\right] &= \left[E_g^{abcy}\right] \end{aligned} \quad (47)$$

In compact form, this is translated as (48).

$$[B]_{sl}^{(abc)} + [C]_{(zsl)}^{(abc)}\left[I_{(nne)_{sl}}\right]^{(abc)} = [E_g]^{(abc)} \quad (48)$$

where

$$[B]_{sl}^{(abc)} = \left|\begin{bmatrix} V_{sl}^{abcx} \\ V_{sl}^{abcy} \end{bmatrix}\right|; \left[I_{(nne)_{sl}}\right]^{(abc)} = \left|\begin{bmatrix} I_{sl}^{abcy} \\ I_{sl}^{abcx} \end{bmatrix}\right| \quad (49)$$

$$[C]_{(zsl)}^{(abc)} = \begin{bmatrix} -\left[Z_{sl}^{abcy}\right] & \left[Z_{sl}^{abcx}\right] \\ \left[Z_{sl}^{abcx}\right] & \left[Z_{sl}^{abcy}\right] \end{bmatrix} \quad (50)$$

In expanded form, the expression (50) can be written as:

$$[C]_{(zsl)}^{(abc)} = \begin{bmatrix} -\begin{bmatrix} Z_{sl}^{aay} & Z_{sl}^{aby} & Z_{sl}^{acy} \\ Z_{sl}^{bay} & Z_{sl}^{bby} & Z_{sl}^{bcy} \\ Z_{sl}^{cay} & Z_{sl}^{cby} & Z_{sl}^{ccy} \end{bmatrix} & \begin{bmatrix} Z_{sl}^{aax} & Z_{sl}^{abx} & Z_{sl}^{acx} \\ Z_{sl}^{bax} & Z_{sl}^{bbx} & Z_{sl}^{bcx} \\ Z_{sl}^{cax} & Z_{sl}^{cbx} & Z_{sl}^{ccx} \end{bmatrix} \\ \begin{bmatrix} Z_{sl}^{aax} & Z_{sl}^{abx} & Z_{sl}^{acx} \\ Z_{sl}^{bax} & Z_{sl}^{bbx} & Z_{sl}^{bcx} \\ Z_{sl}^{cax} & Z_{sl}^{cbx} & Z_{sl}^{ccx} \end{bmatrix} & \begin{bmatrix} Z_{sl}^{aay} & Z_{sl}^{aby} & Z_{sl}^{acy} \\ Z_{sl}^{bay} & Z_{sl}^{bby} & Z_{sl}^{bcy} \\ Z_{sl}^{cay} & Z_{sl}^{cby} & Z_{sl}^{ccy} \end{bmatrix} \end{bmatrix} \epsilon\mathbb{R}^{6\times 6} \quad (51)$$

The NNE current equations can be written similarly. For the slack bus, the NNE current term, $[A]_{sl}^{(abc)}$, used for the augmentation of the $[Y_{Stamp}]$ to generate $[Y_{AugStamp}]$ is as given in (52).

$$[A]_{sl}^{(abc)} = \begin{bmatrix} \begin{bmatrix} 1 & & \\ & 1 & \\ & & 1 \end{bmatrix} & [O_{3\times 3}] \\ [O_{3\times 3}] & \begin{bmatrix} 1 & & \\ & 1 & \\ & & 1 \end{bmatrix} \end{bmatrix} \tag{52}$$

Furthermore, consider a three single-phase transformer bank configured in delta-grounded wye arrangement. We also assume that parameters are given in actual values and that the leakage impedance is placed on the secondary winding of the transformer. Also, consider that the transformer is connected between nodes 'mâĂŹ and 'nâĂŹ of the test network and has effective turns ratio λ. Consequently, the transformer voltage descriptive equation can be written thus (53).

$$[B]_{m}^{(abc)}\,[V]_{m}^{(abc)} + [B]_{n}^{(abc)}\,[V]_{n}^{(abc)} + [C]_{mn}^{(abc)}\,[I]_{TX}^{(abc)} \tag{53}$$

where

$$[B]_{m}^{(abc)} = \begin{bmatrix} \begin{bmatrix} 1 & -1 & \\ & 1 & -1 \\ -1 & & 1 \end{bmatrix} & [O_{3\times 3}] \\ [O_{3\times 3}] & \begin{bmatrix} 1 & -1 & \\ & 1 & -1 \\ -1 & & 1 \end{bmatrix} \end{bmatrix} \tag{54}$$

$$[B]_{n}^{(abc)} = \begin{bmatrix} -\begin{bmatrix} \lambda_a & & \\ & \lambda_b & \\ & & \lambda_c \end{bmatrix} & [O_{3\times 3}] \\ [O_{3\times 3}] & -\begin{bmatrix} \lambda_a & & \\ & \lambda_b & \\ & & \lambda_c \end{bmatrix} \end{bmatrix} \tag{55}$$

$$[C]_{mn}^{(abc)} = \begin{bmatrix} C_1 & C_2 \\ C_3 & C_4 \end{bmatrix} \epsilon \mathbb{R}^{6\times 6} \tag{56}$$

where if no coupling between the three single-phase transformer bank, then:

$$C_1 = \text{diag}\begin{vmatrix} \lambda_a^2 Z_a^y \\ \lambda_b^2 Z_b^y \\ \lambda_c^2 Z_c^y \end{vmatrix}; C_2 = -\text{diag}\begin{vmatrix} \lambda_a^2 Z_a^x \\ \lambda_b^2 Z_b^x \\ \lambda_c^2 Z_c^x \end{vmatrix} \tag{57}$$
$$C_3 = C_2; C_4 = -C_1$$

If couplings exist between the transformer windings, then (57) takes the form of (51). The current flowing in the delta winding (primary-side), $[I]_{TX}^{(abc)}$, is written as (58).

$$[I]_{TX}^{(abc)} = \begin{bmatrix} I_{ab}^y & I_{bc}^y & I_{ca}^y & I_{ab}^x & I_{bc}^x & I_{ca}^x \end{bmatrix}^T \tag{58}$$

The terms required for augmentation in the matrix $[Y_{AugStamp}]$ are derived from (59) and (60).

$$\begin{vmatrix} [I_m^y]^{(abc)} \\ [I_m^x]^{(abc)} \end{vmatrix} = \left[\begin{array}{cc|c} \begin{bmatrix} 1 & & -1 \\ -1 & 1 & \\ & -1 & 1 \end{bmatrix} & & \\ & [O_{3\times 3}] & \\ & & \begin{bmatrix} 1 & & -1 \\ -1 & 1 & \\ & -1 & 1 \end{bmatrix} \end{array}\right] \begin{vmatrix} I_{ab}^y \\ I_{bc}^y \\ I_{ca}^y \\ I_{ab}^x \\ I_{bc}^x \\ I_{ca}^x \end{vmatrix} \tag{59}$$

$$\begin{vmatrix} [I_n^y]^{(abc)} \\ [I_n^x]^{(abc)} \end{vmatrix} = \left[\begin{array}{cc|c} -\begin{bmatrix} \frac{1}{\lambda_a} & & \\ & \frac{1}{\lambda_b} & \\ & & \frac{1}{\lambda_c} \end{bmatrix} & & \\ & [O_{3\times 3}] & \\ & & -\begin{bmatrix} \frac{1}{\lambda_a} & & \\ & \frac{1}{\lambda_b} & \\ & & \frac{1}{\lambda_c} \end{bmatrix} \end{array}\right] \begin{vmatrix} I_{ab}^y \\ I_{bc}^y \\ I_{ca}^y \\ I_{ab}^x \\ I_{bc}^x \\ I_{ca}^x \end{vmatrix} \tag{60}$$

In compact form, (59) and (60) translates to (61) and (62) respectively.

$$\begin{vmatrix} [I_m^y]^{(abc)} \\ [I_m^x]^{(abc)} \end{vmatrix} = [A]_m^{(abc)}\,[I]_{TX}^{(abc)} \tag{61}$$

$$\begin{vmatrix} [I_n^y]^{(abc)} \\ [I_n^x]^{(abc)} \end{vmatrix} = [A]_n^{(abc)}\,[I]_{TX}^{(abc)} \tag{62}$$

where

$$[A]_{m}^{(abc)} = \begin{bmatrix} \begin{bmatrix} 1 & & -1 \\ -1 & 1 & \\ & -1 & 1 \end{bmatrix} & [O_{3\times 3}] \\ [O_{3\times 3}] & \begin{bmatrix} 1 & & -1 \\ -1 & 1 & \\ & -1 & 1 \end{bmatrix} \end{bmatrix} \tag{63}$$

$$[A]_{n}^{(abc)} = \begin{bmatrix} -\begin{bmatrix} \frac{1}{\lambda_a} & & \\ & \frac{1}{\lambda_b} & \\ & & \frac{1}{\lambda_c} \end{bmatrix} & [O_{3\times 3}] \\ [O_{3\times 3}] & -\begin{bmatrix} \frac{1}{\lambda_a} & & \\ & \frac{1}{\lambda_b} & \\ & & \frac{1}{\lambda_c} \end{bmatrix} \end{bmatrix} \tag{64}$$

By observation, it is realised that the relationship in (65) is valid.

$$[A]_{m}^{(abc)} = \left([B]_{m}^{(abc)}\right)^T \tag{65}$$

D. Comparative evaluation of EMANA and MANA in the context of voltage-controlled node constraint handling

Consider an example system having 2-nodes - k and m. Also, assume that the nodes, k and m are respectively PQ and voltage-controlled nodes respectively. Both nodes also have loads connected. Starting with the generic formulation in (1), an iterative solution algorithm can be written for the MANA and EMANA. We illustrate the difference between the two methods using single-phase alone. Since the m^{th} node is voltage-controlled node, then,

$$|V|_m^2 = \left(V_m^r\right)^2 + \left(V_m^i\right)^2 \tag{66}$$

In the MANA formulation, $V_m^r = \sqrt{|V|_m^2 - \left(V_m^i\right)^2}$ is introduced in (1). The resulting formulation will be of the form in (67).

$$\triangle \begin{bmatrix} V_k^r \\ V_k^i \\ V_m^i \\ Q_{g(m)} \end{bmatrix}^{(b)} = \begin{bmatrix} * & * & * & 0 \\ * & * & * & 0 \\ * & * & * & * \\ * & * & * & * \end{bmatrix}^{-1} \times F_G\left(X^{(b)}\right) \tag{67}$$

where the starred $(*)$ entries denote the appropriate partial derivatives in the Jacobian matrix.

In the EMANA however, (66) is used for augmentation of $F_G(X)$ thus yielding $\begin{bmatrix} F_G(X) & F_{pv}(V_m^r, V_m^i) \end{bmatrix}^T$. The resulting formulation will take the form shown in (68).

$$\triangle \begin{bmatrix} V_k^r \\ V_k^i \\ V_m^r \\ V_m^i \\ Q_{g(m)} \end{bmatrix}^{(b)} = \begin{bmatrix} * & * & * & * & 0 \\ * & * & * & * & 0 \\ * & * & * & * & * \\ * & * & * & * & * \\ 0 & 0 & * & * & 0 \end{bmatrix}^{-1} \times \begin{bmatrix} F_G\left(X^{(b)}\right) \\ F_{pv}\left(X^{(b)}\right) \end{bmatrix} \quad (68)$$

The handling of the voltage-controlled node based on reactive power support from DGs is the key difference between MANA and EMANA.

REFERENCES

[1] R. Kang and M. McCulloch, "Identification of electric power system stress through feeder voltage measurement," in *Innovative Smart Grid Technologies Conference Europe (ISGT-Europe), 2014 IEEE PES*. IEEE, 2014, pp. 1–6.

[2] P.-H. Li and S. Pye, "Assessing the benefits of demand-side flexibility in residential and transport sectors from an integrated energy systems perspective," *Applied energy*, vol. 228, pp. 965–979, 2018.

[3] A. internationale de l'énergie and I. Staff, *Cool appliances: policy strategies for energy-efficient homes*. OECD publishing, 2003.

[4] N. Gudi, L. Wang, and V. Devabhaktuni, "A demand side management based simulation platform incorporating heuristic optimization for management of household appliances," *International Journal of Electrical Power & Energy Systems*, vol. 43, no. 1, pp. 185–193, 2012.

[5] X. Liu, A. Aichhorn, L. Liu, and H. Li, "Coordinated control of distributed energy storage system with tap changer transformers for voltage rise mitigation under high photovoltaic penetration," *IEEE Transactions on Smart Grid*, vol. 3, no. 2, pp. 897–906, 2012.

[6] V. Calderaro, V. Galdi, F. Lamberti, and A. Piccolo, "A smart strategy for voltage control ancillary service in distribution networks," *IEEE Transactions on Power Systems*, vol. 30, no. 1, pp. 494–502, 2015.

[7] W. F. Tinney and C. E. Hart, "Power flow solution by newton's method," *IEEE Transactions on Power Apparatus and systems*, no. 11, pp. 1449–1460, 1967.

[8] K. Balamurugan and D. Srinivasan, "Review of power flow studies on distribution network with distributed generation," in *Power Electronics and Drive Systems (PEDS), 2011 IEEE Ninth International Conference on*. IEEE, 2011, pp. 411–417.

[9] D. J. Tylavsky, P. E. Crouch, L. F. Jarriel, J. Singh, and R. Adapa, "The effects of precision and small impedance branches on power flow robustness," *IEEE Transactions on Power Systems*, vol. 9, no. 1, pp. 6–14, 1994.

[10] F. Therrien, I. Kocar, and J. Jatskevich, "A unified distribution system state estimator using the concept of augmented matrices," *IEEE Transactions on Power Systems*, vol. 28, no. 3, pp. 3390–3400, 2013.

[11] V. M. da Costa, N. Martins, and J. L. R. Pereira, "Developments in the newton raphson power flow formulation based on current injections," *IEEE Transactions on power systems*, vol. 14, no. 4, pp. 1320–1326, 1999.

[12] P. A. Garcia, J. L. R. Pereira, S. Carneiro, V. M. da Costa, and N. Martins, "Three-phase power flow calculations using the current injection method," *IEEE Transactions on Power Systems*, vol. 15, no. 2, pp. 508–514, 2000.

[13] M. J. Alam, K. Muttaqi, and D. Sutanto, "A three-phase power flow approach for integrated 3-wire mv and 4-wire multigrounded lv networks with rooftop solar pv," *IEEE Transactions on Power Systems*, vol. 28, no. 2, pp. 1728–1737, 2013.

[14] S. Carneiro, J. L. Pereira, and P. A. N. Garcia, "Unbalanced distribution system power flow using the current injection method," in *Power Engineering Society Winter Meeting, 2000. IEEE*, vol. 2. IEEE, Conference Proceedings, pp. 946–950.

[15] D. Penido, L. Araujo, J. Pereira, P. Garcia, and S. Carneiro, "Four wire newton-raphson power flow based on the current injection method," in *Power Systems Conference and Exposition, 2004. IEEE PES*. IEEE, Conference Proceedings, pp. 239–242.

[16] G. Chang, S. Chu, and H. Wang, "An improved backward/forward sweep load flow algorithm for radial distribution systems," *IEEE Transactions on Power Systems*, vol. 22, no. 2, pp. 882–884, 2007.

[17] I. Kocar and J.-S. Lacroix, "Implementation of a modified augmented nodal analysis based transformer model into the backward forward sweep solver," *IEEE Transactions on Power Systems*, vol. 27, no. 2, pp. 663–670, 2012.

[18] W. H. Kersting, "Center-tapped transformer and 120-/240-v secondary models," *IEEE transactions on industry applications*, vol. 45, no. 2, pp. 575–581, 2009.

[19] P. A. N. Garcia, J. L. R. Pereira, and S. Carneiro, "Voltage control devices models for distribution power flow analysis," *IEEE Transactions on Power Systems*, vol. 16, no. 4, pp. 586–594, 2001.

[20] T.-H. Chen and N.-C. Yang, "Loop frame of reference based three-phase power flow for unbalanced radial distribution systems," *Electric power systems research*, vol. 80, no. 7, pp. 799–806, 2010.

[21] R. A. Jabr, "Radial distribution load flow using conic programming," *IEEE transactions on power systems*, vol. 21, no. 3, pp. 1458–1459, 2006.

[22] R. Singh, B. C. Pal, R. A. Jabr, and P. D. Lang, "Distribution system load flow using primal dual interior point method," in *Power System Technology and IEEE Power India Conference, 2008. POWERCON 2008. Joint International Conference on*. IEEE, 2008, pp. 1–5.

[23] P. A. Garcia, J. Pereira, S. Carneiro, M. P. Vinagre, and F. V. Gomes, "Improvements in the representation of pv buses on three-phase distribution power flow," *IEEE Transactions on Power Delivery*, vol. 19, no. 2, pp. 894–896, 2004.

[24] I. Kocar, J. Mahseredjian, U. Karaagac, G. Soykan, and O. Saad, "Multiphase load-flow solution for large-scale distribution systems using mana," *IEEE Transactions on Power Delivery*, vol. 29, no. 2, pp. 908–915, 2014.

[25] O. S. Nduka and B. C. Pal, "Harmonic domain modeling of pv system for the assessment of grid integration impact," *IEEE Transactions on Sustainable Energy*, vol. 8, no. 3, pp. 1154–1165, 2017.

[26] O. Nduka and B. Pal, "Quantitative evaluation of actual loss reduction benefits of a renewable heavy dg distribution network," *IEEE Transactions on Sustainable Energy*, vol. 9, no. 3, pp. 1384–1396, 2018.

[27] L. Wedepohl and L. Jackson, "Modified nodal analysis: an essential addition to electrical circuit theory and analysis," *Engineering Science and Education Journal*, vol. 11, no. 3, pp. 84–92, 2002.

[28] J. Vlach, "Network theory and cad," *IEEE Transactions on Education*, vol. 36, no. 1, pp. 23–27, 1993.

[29] J. Vlach and K. Singhal, *Computer methods for circuit analysis and design*. Springer Science and Business Media, 1983.

[30] B. Stott, "Effective starting process for newton-raphson load flows," in *Proceedings of the institution of electrical engineers*, vol. 118, no. 8. IET, 1971, pp. 983–987.

[31] F. Therrien, M. Belletête, J.-S. Lacroix, and M. J. Reno, "Algorithmic aspects of a commercial-grade distribution system load flow engine," in *2017 IEEE 44th Photovoltaic Specialist Conference (PVSC)*. IEEE, 2017, pp. 1579–1584.

[32] R. Ebrahimian and R. Baldick, "State estimator condition number analysis," *IEEE Transactions on Power Systems*, vol. 16, no. 2, pp. 273–279, 2001.

[33] Y. P. Agalgaonkar, B. C. Pal, and R. A. Jabr, "Distribution voltage control considering the impact of pv generation on tap changers and autonomous regulators," *IEEE Transactions on Power Systems*, vol. 29, no. 1, pp. 182–192, 2013.

[34] R. Singh, B. C. Pal, and R. A. Jabr, "Statistical representation of distribution system loads using gaussian mixture model," *IEEE Transactions on Power Systems*, vol. 25, no. 1, pp. 29–37, 2010.

[35] S. Xu, J. Zhang *et al.*, "A new data mining approach to predicting matrix condition numbers," *Communications in Information & Systems*, vol. 4, no. 4, pp. 325–340, 2004.

[36] W. H. Press, S. A. Teukolsky, W. T. Vetterling, and B. P. Flannery, *Numerical recipes 3rd edition: The art of scientific computing*. Cambridge university press, 2007.

[37] T. Young and M. J. Mohlenkamp, "Introduction to numerical methods and matlab programming for engineers," *Department of Mathematics, Ohio University*, 2014.

Onyema S. Nduka (S'14-M'18) is currently a post-doctoral research associate at the control and power group of Imperial College London. He received the BEng degree in Electrical and Electronic Engineering (specializing in Power systems Engineering Technology) from Federal University of Technology, Owerri, Nigeria, in 2011. He also obtained an MSc degree in Control Systems and a PhD in Electrical Engineering from Imperial College London, UK, in 2014 and 2018 respectively.

He is a COREN registered Electrical Engineer and a certified PRINCE2 practitioner. His research interests include distribution systems and microgrid planning and operation, power quality, and low-carbon technology (including PVs, small-scale energy storage and electric vehicles) integration into smart grids.

Yue Yu received the B.Sc. degrees in electrical engineering from University of Bath, UK and North China Electric Power University, China, in 2015, and M.Sc. degree in advanced electrical machines, power electronics and drives from University of Sheffield, UK, in 2016. He is currently working towards the PhD degree at Imperial College London, UK. His research interests include modelling, control and optimization of DC microgrid with integration of electric vehicle fleet.

Bikash C. Pal (M'00-SM'02-F'13) received B.E.E. (with honors) degree from Jadavpur University, Calcutta, India, M.E. degree from the Indian Institute of Science, Bangalore, India, and Ph.D. degree from Imperial College London, London, U.K., in 1990, 1992, and 1999, respectively, all in electrical engineering.

Currently, he is a Professor in the Department of Electrical and Electronic Engineering, Imperial College London. His current research interests include renewable energy modelling and control, state estimation, and power system dynamics.

He is Vice President Publications, IEEE Power & Energy Society. He was Editor-in-Chief of IEEE Transactions on Sustainable Energy (2012-2017) and Editor-in-Chief of IET Generation , Transmission and Distribution (2005-2012) and is a Fellow of IEEE for his contribution to power system stability and control.

Ephraim N.C. Okafor is a professor of Electrical Power Systems at the Federal University of Technology, Owerri, Nigeria, and a registered Electrical Engineer with the Council for Regulation of Engineering in Nigeria (COREN).